Opposing roles of blood-borne monocytes and tissue-resident macrophages in limbal stem cell damage

Chengxin Zhou*[1,2,3], Fengyang Lei*[1,2,3], Mirja Mittermaier[1], Bruce Ksander[1], Reza Dana[1], Claes H. Dohlman[1,2], Demetrios G. Vavvas[4], James Chodosh[1,2,3], Eleftherios I. Paschalis† [1,2,3]

[1]Department of Ophthalmology, Massachusetts Eye and Ear and Schepens Eye Research Institute, Mass. General Brigham, Harvard Medical School, Boston, MA

[2]Boston Keratoprosthesis Laboratory, Department of Ophthalmology, Massachusetts Eye and Ear, Mass. General Brigham, Harvard Medical School, Boston, MA

[3]Disruptive Technology Laboratory, Department of Ophthalmology, Massachusetts Eye and Ear, Harvard Medical School, Boston, MA

[4]Retina Service, Department of Ophthalmology, Massachusetts Eye and Ear, Mass. General Brigham, Harvard Medical School, Boston, MA

* Equal contribution

†**Corresponding author and reprints:** Eleftherios I. Paschalis, Department of Ophthalmology, Massachusetts Eye and Ear and Schepens Eye Research Institute, 20 Staniford St. Boston, MA 02114, USA; e-mail: eleftherios_paschalis@meei.harvard.edu

Key Words: Limbal stem cell deficiency, cornea, epithelium, macrophages, monocytes, inflammation

Running title: Secondary inflammatory damage to Limbal Stem Cells

Abstract

Limbal stem cell (LSC) deficiency is a frequent and severe complication after chemical injury to the eye. Previous studies have assumed that this is mediated directly by the injury. Here we show that LSC loss occurs through immune cell mediators, even without direct injury to LSCs. In particular, elevation of anterior chamber (AC) pH causes acute uveal stress, release of inflammatory cytokines at the basal limbal tissue, and subsequent LSC death. Peripheral $CCR2^{+}$ $CX3CR1^{-}$ monocytes are key mediators through the upregulation of tumor necrosis factor alpha (TNF-α) at the limbus, which in turn causing LSC death. In contrast to peripherally-derived monocytes, $CX3CR1^{+}$ $CCR2^{-}$ tissue-resident macrophages have a protective role and their pharmacological depletion prior to injury exacerbates LSC loss and increases LSC vulnerability to apoptosis following exposure to TNF-α. This, despite the reduced number of $CCR2^{+}$ cell infiltration into the tissue. Consistently, repopulation of the cornea by new tissue-resident macrophages after depletion restores their M2-like polarization upon exposure to rTNF-α and suppresses LSC inflammatory cell death. This findings may have clinical implication in patient with chemical burns.

Significance

Limbal stem cell (LSC) loss after chemical burn is a significant clinical problem that has long been thought to be the result of direct chemical injury. This study demonstrates the existence of competing inflammatory mechanism responsible for LSC death, mediated by infiltrating peripheral monocytes that antagonize and overcome the protective role of tissue-resident

macrophages. Thus, enhancing the role of tissue-resident macrophages while suppressing that of infiltrating monocytes could be a novel therapeutic strategy for LSC survival.

Introduction

Ocular chemical injury can lead to corneal blindness even if promptly treated[1]. One of the most important anatomic structures affected by the injury is the limbal basal layer[2], which contains a unique population of stem cells, responsible of maintaining and replenishing the corneal epithelium[3]. Complete damage to the limbal niche results in limbal stem cell (LSC) deficiency, loss of corneal transparency, and subsequent vision loss[4]. LSC transplantation can help restore vision, but long-term results are hampered by gradual loss of donor cells and gradual loss of corneal transparency[5, 6]. Therefore, preserving viable LSCs can help restore corneal epithelium and provide the required donor cells for subsequent expansion and auto-graft.

Until now, LSC damage after alkali injury has been attributed to the direct damage by the caustic agent[7]. However, recently we have seen significant LSC loss occurring even in absence of direct contact with the agent[8-10]. Here we show that secondary inflammation is an alternative mechanism of LSC loss in the absence of direct damage by the caustic agent. Mechanistically, this process is instigated by rapid pH and oxygen changes in the anterior chamber that cause acute uveal stress and subsequent recruitment of inflammatory monocytes, especially at the basal limbal tissue. Recruited monocytes secrete tumor necrosis factor alpha (TNF-α) which initiates programmed cell death at the limbus. In contrast, tissue-resident macrophages are protective; in the setting of injury, tissue-resident macrophage depletion exacerbates monocyte infiltration, TNF-α release and subsequent LSC loss. Moreover, tissue resident macrophage depletion augments LSC susceptibility to TNF-α-mediated apoptosis *ex vivo*. Interestingly, repopulation of the corneal by new tissue-residue macrophages after depletion restore the protective phenotype of corneal macrophages and prevents LSC loss following injury. These findings shed light on the

complex physiological and immunological mechanisms of LSC loss and highlight the important immunoregulatory role of tissue-resident macrophages and the detrimental role of peripheral monocytes in LSC preservation.

Results

Limbal stem cell damage does not require contact with the caustic agent.

To investigate whether LSC damage occurs even in the absence of direct injury to the limbus, we created central corneal alkali injuries in rabbits and mice. In this model, the peripheral cornea and limbus remains unaffected by the caustic agent **(Fig. 1A)**. Central corneal alkali injury in the rabbit eye caused significant cell death beyond the affected area, which extended to the peripheral cornea and limbus **(Fig. 1 B-D)**. There was evidence for ongoing cell death by apoptosis in both limbal epithelial and stromal cells, even 2 weeks after the injury, as indicated by TUNEL assay (**Fig. 1 B, D**), and as compared to the naive rabbit eyes (**Fig. 1 C,D**). The damage to the limbus resulted in extensive neovascularization and conjunctivalization of the corneal surface within 2 weeks and dilation of the limbal vessels **(Fig. 1 E, F)**. Moreover, similar results were obtained in the mouse **(Fig. 1 G-O)**.

Limbal stem cell damage after central cornea burn is mediated by pH elevation in the anterior chamber.

Previous studies have shown that corneal alkali injury causes rapid aqueous humor pH elevation from 7.4 to 11.4, within seconds, resulting in inflammation of the uvea[9]. To investigate the contribution of aqueous humor pH elevation to LSC loss, independently of ocular

surface injury, we performed controlled elevation of the aqueous humor pH by anterior chamber (AC) cannulation of 4 µL of balanced salt solution (BSS) adjusted to a pH 11.4.

Cannulation of the AC with 11.4 pH caused severe neovascularization and conjunctivalization of the cornea, iris pigment dispersion and deposition onto the posterior surface of the cornea, and pupil margin deformation **(Fig. 2 A)**. Cannulated eyes with 11.4 pH solution exhibited complete loss of ABCB5^{+} expression, a marker of limbal epithelial stem cells, [11] by 3 months, as assessed by confocal microscopy **(Fig. 2 B, C, G)**, suggesting a complete loss of limbal epithelial stem cells. In contrast, eyes cannulated with normal (7.4) pH solution did not exhibit pathologic changes in the AC or iris, and the cornea remained avascular and transparent as assessed one month after the procedure **(Fig. 2 D)**. As expected, cannulated eyes with 7.4 pH solution retained a normal population of ABCB5^{+} limbal epithelial stem cells at the limbus, as assessed at 3 months **(Fig. 2 E, F, G)**. This model did not cause chemical injury to the corneal surface. Representative photo of the cannulation procedure **(Fig. 2 H)**.

Peripheral inflammatory monocyte contribute to limbal stem cell damage after injury.

The role of inflammatory monocytes in LSC damage was evaluated using the double reporter CX3CR1$^{+/EGFP}$::CCR2$^{+/RFP}$ mouse model[12] by *in situ* hybridization and protein tissue analysis. Typically, interstitial and tissue-resident macrophages express CX3CR1, while circulating inflammatory monocytes express CCR2[12, 13].

Within 24 hours of a central corneal alkali injury, a significant number (17.4%) of CD45^{+} cells infiltrated into the corneal/limbus **(Fig. 3 A-B)**. This was associated with increase in the number of CCR2^{+} cells from 0.04% to 5.3% and of CX3CR1^{+} cells from 0.06% to 1.3% within

24 hours **(Fig. 3 B, C)**. By day 7, the number of the CCR2^{+} cells was disproportionally higher compared to the CX3CR1^{+} tissue-resident macrophages in the injured cornea, as shown by representative confocal images and quantification of the CX3CR1$^{+/EGFP}$ and CCR2$^{+/RFP}$ cells in the cornea/limbus **(Fig. 3 D-F)**. In naive mice, the cornea was predominantly occupied by ramified CX3CR1$^{+/EGFP}$ cells with scant CCR2$^{+/RFP}$ cells present across the corneal tissue **(Fig. 3 D, F)**. Seven days after the alkali injury the number of CCR2$^{+/RFP}$ cells was significantly higher compared to naive eyes **(Fig. 3 E, F)** with a high number of CX3CR1$^{+/EGFP}$ cells located primarily at the limbal area (**Fig. 2 E, F**). Quantification of the two immune cell populations in flat-mounts revealed a disproportional increase in CCR2$^{+/RFP}$ cells relative to CX3CR1$^{+/EGFP}$ cells **(Fig. 3 F)**. Abnormal influx of inflammatory cells in the limbus was also observed in rabbit eyes after central corneal burn, characterized by CD45^{+} myeloid cell infiltration in the basal limbal tissue, which remained present even 3 months after the injury **(Fig. 3 G-I)**.

Previous studies have revealed that TNF-α is upregulated after chemical injury[14-16]. By using flow cytometry were quantified the contribution of CX3CR1^{+} tissue-resident macrophages and CCR2^{+} peripheral monocytes in TNF-α release 24 hours of the injury. Infiltrating CCR2^{+} CX3CR1^{-} monocytes contributed significantly in the TNF-α secretion in the tissue, as compared to the CX3CR1^{+} CCR2^{-} tissue-resident macrophages which showed minimal contribution **(Fig. 4 A-C)**. By using *in situ* hybridization and protein analysis we showed that TNF-α mRNA and protein expression was significantly upregulated at the site of injury (central cornea) and in the basal limbal tissue harboring the LSCs, but not in the intervening peripheral cornea (**Fig. 4 D-M)**.

Tissue-resident macrophages are key regulators of limbal stem cell protection during injury.

To understand the differential role of peripheral and the tissue-resident monocytes/ macrophages in LSC damage, we employed a bone marrow CX3CR1$^{+/EGFP}$::CCR2$^{+/RFP}$ chimera model to fate map infiltrating monocytes/macrophages in the cornea and to study their specific contribution in LSC damage[13, 17, 18].

In naive BMT CX3CR1$^{+/EGFP}$ ::CCR2$^{+/RFP}$ mice, the cornea was predominantly populated by CX3CR1^{+} tissue-resident macrophages, with sparse blood-derive CCR2^{+} monocytes distributed around the limbus **(Fig. 5 A, F)**. Corneal alkali injury in BMT mice triggered CCR2$^{+/RFP}$ cell infiltration from the blood into the cornea and limbus **(Fig. 5 B, F 'Injured')** which resulted in significant limbal epithelial cells apoptosis within 24 hours **(Fig. 5 H, L)**. To understand the role of CX3CR1$^{+/EGFP}$ tissue-resident macrophages in limbal stem cell damage, BMT mice at steady-state were treated with CSF1R inhibitor (PLX5622) to eliminate tissue-resident CX3CR1$^{+/EGFP}$ macrophages **(Fig. 5 C-F)**. Indeed, CSF1R inhibition was able to deplete all tissue-resident macrophages of the cornea, confirming previously studies in tissue resident macrophages of other tissues[13, 17, 19, 20]. However, CSF1R inhibition did not affect the number of peripheral CCR2^{+} that infiltrated the cornea and limbus within 24 hours of the injury ('PLX+Injury'), **(Fig. 5 C, F)**. Importantly, depletion of tissue-resident macrophages exacerbated limbal epithelial cell apoptosis after injury, as compared to injured mice with intact tissue-resident macrophages **(Fig. 5 H, I, L)**. Further studies showed that this effect was not attributed to the CSF1R inhibitor, which in the absence of ocular injury did not cause limbal epithelial cell apoptosis or recruitment of peripheral CCR2^{+} monocyte into the tissue **(Fig. 5 D, J, L)**.

To further assess the protective role of tissue-resident macrophages we performed additional experiments in which macrophage depleted mice were allowed to achieve tissue-resident macrophage repopulation by stopping the administration of CSF1R inhibitor for 2 months **(PLX off (2m))**. Cessation of CSF1R inhibitor re-established normal tissue-resident macrophages in the cornea and restored their protective role against limbal epithelial cell apoptosis **(Fig. 5 E, K, L)**.

Depletion of tissue-resident macrophages sensitizes LSCs to TNF-α

To further understand the role of tissue-resident macrophages in suppressing immune-mediated LSC damage, corneal tissues from wild-type mice that were treated with CSF1R inhibitor for 3 weeks were explanted and co-cultured for 6 hours in KSFM+10% FBS medium supplemented with 5ng/mL murine recombinant TNF-α. Macrophage depletion increased the susceptibility of limbal epithelial cell to TNF-α induced apoptosis from 3.7% (wild-type mice) to 32% (PLX treated mice), **(Fig. 5 M, N)**, suggesting that tissue-resident macrophages are important modulators of LSC susceptibility to TNF-α. This hypersensitivity of limbal epithelial cells to apoptosis after depletion of tissue-resident macrophages was not attributed to *ex vivo* culture condition or to primary cytotoxicity of the rTNF-α, as both were well tolerated and caused minimal or no apoptosis to the limbus in mice with intact macrophages **(Fig. 5 M, N)**. Instead, it was attributed to the loss of the protective/reparative function of tissue-resident macrophages and their implication in regulating inflammation. Indeed, flow cytometric analysis of explanted corneal/limbal tissues demonstrated a switch in the polarization of tissue-resident macrophages from classically activated, M1 pro-inflammatory phenotype to an alternatively

activated M2 anti-inflammatory phenotype upon exposure to rTNF-α *ex vivo*, as defined by the down-regulation of MHC-II^{hi} and CD86^{hi} and the upregulation of CD206^{hi} surface markers **(Fig. 6 A, B, CTRL & CTRL+rTNF-α)**. This phenotype was abolished in mice theater with CSF1R inhibitor for 3 weeks *in vivo* prior to exposure to rTNF-α *ex vivo*, **(Fig. 6, A, B - PLX & PLX+rTNF-α)**. Interestingly, cessation of the inhibitor for 2 months led to repopulation of cornea with new tissue-resident macrophages that re-established the macrophages M2-like polarization upon exposure to rTNF-α *ex vivo* **(Fig. 6, PLX OFF 2M , PLX OFF 2M+rTNF-α)**.

DISCUSSION

Limbal stem cell deficiency, a common and frequent complication after ocular chemical burn. Previous studies have assumed that LSC loss is caused either by direct damage from the caustic agent or from limbal ischemia due to vascular damage, or both[21]. Here we show that LSC loss is not mediated exclusively by these two mechanisms, but also through physiological changes within the anterior chamber that cause an immune response in the uvea. We demonstrate that rapid pH elevation in the aqueous humor cause acute uveal stress and subsequent infiltration of peripheral monocytes into the basal limbal tissue **(Fig. 7)**. In contrast, tissue-resident macrophages suppress inflammatory damage to the LSCs, whereas their depletion exacerbates LSC loss.

In previous studies we have shown that corneal alkali burns cause a rapid increase in anterior chamber pH from 7.4 to 11.5 within seconds[9]. Here we expand on this finding and show that direct AC pH elevation, without ocular surface burn, contributes to LSC damage

independent of the physical damage to the ocular surface. Although cells can survive such transient pH elevation[22], subsequent stress to the uvea activates an inflammatory response that damages the LSCs. Key cellular mediators in this process are the peripheral CCR2^{+} monocytes, that infiltrate the tissue, especially around the limbus. This process is independent of the actual physical damage to the surface; artificial elevation of the aqueous humor pH with cannulation causes a similar immune activation, LSC loss, and conjunctivalization of the cornea. To our knowledge, this is the first study to demonstrate that pH elevation in the anterior chamber is an important cause of LSC loss in ocular surface alkali injury.

The limbal niche is supported by the presence of a distinct vasculature with radially oriented hairpin loops of arteries and veins(23), derived from the palisades of Vogt. These vessels provide the stem cells with nutrition and various blood-borne substances that support the LSCs[24, 25]. Owing to the distinct anatomical location of the limbus, LSCs are exposed to interactions with immune cells, and therefore, susceptible to damage induced by inflammatory mediators[26, 27]. Our results suggest that resident macrophages protect LSCs from destructive infiltrating cells or secretion of inflammatory mediators, but in extreme situations of stress, this protective effect is overwhelmed by vast infiltration of immune cells and the production of inflammatory cytokines at the limbal area. Although we demonstrated the opposing roles of tissue-resident macrophages and infiltrated peripheral monocytes in LSC survival, further studies are required to fully characterize the immunological profiles of the two immune cell populations.

Previous studies have shown that tissue-resident macrophages have an anti-inflammatory / tissue-repair function during tissue damage[28, 29] as compared to blood-borne CCR2^{+} monocytes that are more pro-inflammatory and contribute to tissue damage[12, 20, 30-35].

Here we show that depletion of the tissue-resident macrophages increased LSC susceptibility to apoptosis following exposure to recombinant TNF-α and repopulation of the cornea by new tissue-resident macrophages after depletion restores the protective function and ameliorates LSC loss. This is corroborated by data showing that tissue-resident macrophages contribute minimally to TNF-α release, as compared to $CCR2^{+}$ cells from periphery, and following exposure to TNF-α, tissue-resident macrophages switch from classical to alternative activation. Since short (1 week) [18] or long-term (3 weeks)[17] inhibition of CSF1R can affect a variety of other immune cells[17, 18, 36], we employed an *ex vivo* model to study the role of tissue-resident macrophages in the absence of peripheral immune cell infiltration. Our experiments suggest that tissue-resident macrophages undergo phenotype switch following exposure to TNF-α from classically activated M1 pro-inflammatory to alternatively activated M2 anti-inflammatory, as defined by the down-regulation of MHC-II^{hi} and $CD86^{hi}$ and the upregulation of $CD206^{hi}$ surface markers. Interestingly, this phenotype is abolished in mice treated with CSF1R inhibitor, however, cessation of the inhibitor for 2 months allows repopulation of the cornea with new tissue-resident macrophages and restore their ability to polarize to M2-like phenotype upon exposure to rTNF-α *ex vivo*. This suggest that tissue-resident macrophages of the cornea can be repopulated by the blood to provide important regulatory functions tissue support. This finding aligns with recent publications showing that tissue-resident macrophages in other tissues play a protective rather than deleterious role[9, 13, 17, 20, 37]. This is an important finding supporting the important regulatory role of tissue-resident macrophages in corneal immunology and LSC survival. Conversely, we show that the peripherally infiltrating $CCR2^{+}$ cells mediate the damage to the LSC and as such, suppression of the CCR2-axis should be the therapeutic target.

In conclusion, preserving the corneal limbal epithelium after severe chemical injury has important ramifications for patients[4, 7, 38-43]. Understanding and controlling the molecular and cellular mechanisms that cause LSC loss can minimize the damage to the ocular surface and improve the success rate of adjuvant therapies and surgical approaches. To this end, the CCR2 axis appears to drive the detrimental effects of LSC loss through TNF-α-mediated inflammation, while the tissue-resident CX3CR1 macrophages appear to have a protective and immunoregulatory role against LSC apoptosis. Taking advantage of these finding in a translational manner could help clinical outcomes of LSC deficiently after trauma or inflammatory diseases.

Methods and Materials

Mouse model of corneal alkali injury

All animal procedures were performed in accordance with the Association For Research in Vision and Ophthalmology Statement for the Use of Animals in Ophthalmic and Vision Research, and the National Institutes of Health Guidance for the Care and Use of Laboratory Animals. The study was approved by the Animal Care Committee of the Massachusetts Eye and Ear. C57BL/6, Balb/c, B6.129P-*Cx3cr1*^{tm1Litt}/J (CX3CR1$^{EGFP/EGFP}$ Stock 005582), B6.129(Cg)-*Ccr2*$^{tm2.1Ifc}$/J (CCR2$^{RFP/RFP}$ Stock 017586), B6.129S-*Tnfrsf1a*^{tm1Imx} *Tnfrsf1b*^{tm1Imx}/J (TNFR1/2$^{-/-}$ Stock 003243) mice were obtained from the Jackson Laboratory (Bar Harbor, ME). CX3CR1$^{+/EGFP}$::CCR2$^{+/RFP}$ reporter mice were generated by in-house breeding[9, 12, 13, 20]. Mice between the ages of 6-12 weeks were used for this study.

Corneal alkali injuries were performed as per our published protocol[16]. Briefly, mice were anesthetized using ketamine (60 mg/kg) and xylazine (6 mg/kg). Proparacaine hydrocloride USP 0.5% (Bausch and Lomb, Tampa, FL, USA) eye drop was applied to the cornea 1 minute before the burn. The cornea was carefully dried with a Weck-Cel (Beaver Visitec International, Inc, Waltham, MA, US). A 2 mm diameter filter paper soaked into 1 M sodium hydroxide (NaOH) solution was applied to the central cornea for 20 seconds, avoiding exposure of the peripheral cornea and limbal area. After the injury, the eye was promptly irrigated with sterile saline for 15 minutes. Buprenorphine hydrochloride (0.05 mg/kg) (Buprenex Injectable, Reckitt Benckiser Healthcare Ltd, United Kingdom) was administered subcutaneously for pain alleviation and Polytrim eyedrops (polymyxin B/trimethoprim, Bausch & Lomb Inc, Bridgewater, NJ) were applied to the eye to prevent bacterial infection. Mice were kept on a heating pad until fully awake.

Rabbit model of chemical injury

Six Dutch-Belted female rabbits (Covance, Dedham, MA) between 2 and 2.5 kg were anesthetized by intramuscular injection of ketamine hydrochloride INJ, USP (35 mg/kg), (KetaVed®, VEDCO, St.Joseph, MO) and xylazine (5 mg/kg), (AnaSed®, LLOYD, Shenandoah, Iowa). Topical anesthetic (0.5% proparacaine hydrochloride, Bausch & Lomb, Tampa, Florida) was applied to the operative eye. Corneal alkali injuries were performed using an 8 mm diameter filter paper soaked in 2N NaOH and applied to the central cornea for 10 seconds, followed by immediate eye irrigation with saline solution for 15 minutes. After the burn, yohimbine (0.1mg/ kg), (Yobine®, LLOYD, Shenandoah, Iowa) was administered in a marginal ear vein to reverse

anesthesia. A single dose of buprenorphine (0.03 mg/kg) (Buprenex Injectable, Reckitt Benckiser Healthcare Ltd, United Kingdom) was injected subcutaneously and a transdermal fentanyl patch (12mcg/hour), (LTS Lohmann Therapy System, Corp, NJ) was applied to the skin for 3 days to alleviate pain. Polytrim eyedrops (polymyxin B/trimethoprim, Bausch & Lomb Inc, Bridgewater, NJ) were applied to the eye for 7 days to prevent bacterial infection.

Anterior chamber pH elevation with cannulation.

Anterior chamber pH elevation was achieved by replacing the physiological aqueous humor of mice with an equal volume of balanced salt solution (BSS) adjusted to pH 11.4. pH to match the pH of the anterior chamber of mice and rabbits observed 1 minute after corneal surface injury with NaOH-soaked filter paper[16]. Cannulation was performed using a glass micropipette needle, fitted on a gas-powered microinjection system (MDI, South Plainfield, NJ, USA). The needle was mounted on a 3D stereotaxis device, observed under an ophthalmic surgical microscope (Carl Zeiss Meditec, Thornwood, NY, USA) and inserted into the anterior chamber (AC) through the clear cornea. A volume of 4 µL of aqueous humor was replaced by an equal volume of BSS pH 11.4. After aqueous the humor replacement, the needle was kept in the AC for 5 minutes to prevent a backwards leak though the wound. After removal of the needle, the wound was spontaneously sealed by stromal edema. The site of injection was gently irrigated with normal sterile saline and the eye was tapped with a cotton tip to confirm wound closure.

Monocyte fate mapping using a chimera

C57BL/6J mice were myelodepleted, as previously described[12, 13, 20, 44], with 3 intraperitoneal injections of busulfan (Sigma-Aldrich, St Louis, MO) (35mg/kg) 7, 5, and 3 days

prior to bone marrow transfer. CX3CR1$^{+/EGFP}$::CCR2$^{+/RFP}$ bone marrow cells (5x10^6 total bone marrow cells) were transferred to myelodepleted C57BL/6J mice via tail injection 1 month prior to corneal alkali injury. Bactrim (trimethoprim 80 mg and sulfamethoxazol 400 mg resuspension in 400mL drinking water) was given *ad lib* for 15 days post busulfan treatment.

Tissue-resident macrophage depletion using CSF1R inhibitor

The tissue-resident macrophages of the limbus (and cornea) were depleted with 3-weeks administration of PLX5622 CSF1R inhibitor. The compound was provided by Plexxikon Inc. (Berkeley, CA, USA) and formulated in AIN-76A standard chow by Research Diets Inc. (New Brunswick, NJ, USA). Complete tissue-resident macrophages depletion was achieved with a dose of 1200 ppm, given to the mice for 3 weeks.

***ex vivo* corneal culture experiments**

Eyeballs were enucleated from age-matched C57BL/6J mice (6-8 weeks) that received either 3-weeks diet of AIN-76A standard chow or normal diet. Immediately after euthanasia, eyeballs were enucleated and washed in cold Keratinocyte serum-free medium (KSFM, 17005042, Gibco, Grand Island, US). The cornea and limbus were dissected from each eye and the iris was removed. The tissue was gently washed in cold KSFM and cut into two halves with a surgical blade. Half explants were plated separately in 24-well plates, with epithelium facing upward. After removing excess media around the tissue, the explants were left on ice for 15mins to allow tissue adhesion to the culture plate surface. The attached explants were then cultured in KSFM+10% fetal bovine serum (FBS) at 37^{0}C, 95% humidity, and 5% CO_2 overnight. Culture

media was then changed to KSFM+ 10%FBS +/- murine TNF-α (5ng/mL, 315-01A, PeproTech, Rocky Hill, NJ) the next day, and incubated for 6 hours. For immunohistochemistry, tissues were fixed with 8% Paraformaldehyde solution for 20 minutes and frozen in Optimal Cutting Temperature (OCT) compound (Tissue-Tek 4583, Torrance, CA, USA) on dry ice. For flow cytometry analysis, tissues were digested in Collagenase solution for 1 hour at 37°C (Worthington Biochemical, Lakewood, NJ). Cells were washed once and blocked by Fc Block (Clone: 2.4G2, BD Pharmingen) before staining using a panel of fluorescent labeled antibodies. FACS was performed using BD LSR II and data were analyzed using FlowJo (BD, v10.7).

Immunohistochemical analysis

For whole globes, eyes were fixed using 4% paraformaldehyde (PFA) for 1 hour at room temperature and the frozen in OCT compound on dry ice. Multiple sagittal sections (~10µm in thickness) were obtained from the center and the periphery of the globe. Tissue sections were transferred to positive charged glass slides Superfrost® Plus 75x25mm 1mm thickness (VWR, Radnor, PA, USA) for further processing.

For corneal flat mounts, eyes were first fixed in 4% PFA solution for 1 hour at +4ºC and tissues containing cornea, limbus and conjunctiva were surgically dissected, washed in phosphate buffer solution (PBS) with 0.1% Triton-X100 at +4ºC, and blocked in a buffer containing 5% bovine serum albumin and 0.3% Triton-X100 for 2 hours at +4ºC. Tissues were incubated with appropriate antibodies overnight at +4ºC, washed in PBS and re-incubated with secondary antibodies for 2 hours at room temperature. Tissues were washed again in PBS and transferred to positive charged glass slides Superfrost® Plus 75x25 mm, 1 mm thickness (VWR, Radnor, PA, USA) with the epithelium facing upwards for flat mount imaging. Four relaxing radial incisions

were made to generate 4 flat tissue quadrants. UltraCruzTM mounting medium (sc-24941, Santa Cruz Biotechnology, Santa Cruz, CA) was applied and the tissues were covered by No.1 coverslips and nail polish. The following antibodies were used: Mouse monoclonal anti-TNF-α primary antibody pre-conjugated with FITC (Novus, NBP1-51502) 1:100; Goat polyclonal anti-K12 primary antibody (Santa Cruz, sc-17101) 1:100; Rabbit monoclonal anti-K13 primary antibody (Abcam, Cambridge, MA, USA, ab92551) 1: 200; Mouse monoclonal ABCB5 antibody (M3C2 1: 100; donated from Drs. Markus Frank and Bruce Ksander).

i*n situ* hybridization

Tissue cryosections were fixed in 4% PFA for 1 hour at +4ºC. The slides were serially dehydrated with 50%, 70% and 100% ethanol. Tissue sections were treated with RNAscope (ACD, Newark, CA, USA) hydrogen peroxide for 10 min, followed by 20 min of RNAscope protease IV treatment (Cat. No 322336). Tissue sections were then incubated with different RNAscope probes including target gene probe, negative control probe, and Mm-Ppib positive control probe (ACD, Newark, CA, USA) at 40ºC in a humidified HybEZ oven for 2 hours. 6-step mRNA signal amplification was performed using the RNAscope 2.5 HD Red detection kit, according to manufacturer's protocol. Slides were washed twice in RNAscope wash buffer after each amplification step. mRNA signal was detected with red chromogenic reagent. Tissue sections were counterstained with 50% Hematoxylin solution, and mounted in EcoMount medium (Biocare, Concord, CA, USA) with glass coverslips for image quantification.

Microscopy

Tissue slides were imaged using the Zeiss Axio Imager M2 (Zeiss, Germany) fluorescence microscope with 20X dry and 63X oil immersion objective lenses. Flat-mount tissues were imaged using Leica SP8 confocal microscope (Leica, Microsystems inc, Buffalo Grove, IL, USA). Images were taken using 10x, 20x, 40x and 63x objective lenses and by performing z- axial scanning of 0.7, 0.6, 0.4 and 0.3 µm step size, respectively. ImageJ was used to obtain maximum and average projections of the z-axis image stacks. Amira (Thermo Scientific™, Hillsboro, Oregon, USA), 3-D rendering software was used to generate volumetric images and color-coded depth maps. Corneal tissue-resident macrophages were quantified using z-stack projections and volumetric 3-D analysis.

Flow cytometry

Tissues were harvested at different time points and treated with collagenase Type I dissociation system (Worthington, Lakewood, NJ, USA) for subsequent flow cytometry. Different fluorescent antibodies against CD45 (Clone: 104), CD11b (Clone: M1/70), I-A/I-E (MHC-II) (Clone: M5/114.15.2), C-X_3-C motif chemokine receptor 1 (CX3CR1; Clone: SA011F11), CD86 (clone: GL-1), CD206 (clone: C068C2), (Biolegend, San Diego, CA, USA) were used to identify cell markers. Approximately 6% of the corneal cells were analyzed using the BD LSR II cytometer (BD Biosciences, San Jose, CA) and flow data were processed using the FlowJo software version 10.6.2 (Tree Star, Ashland, OR, USA). $CX3CR1^{+}$ and C-C motif chemokine receptor 2 positive ($CCR2^{+}$) cells in $CX3CR1^{+/EGFP}$::$CCR2^{+/RFP}$ double reporter or chimeras were quantified using endogenous $EGFP^{+}$ and RFP^{+} expression, respectively.

TUNEL labeling and quantitation of DNA fragmentation.

TUNEL labeling was performed in tissue sections using the Roche TUNEL kit (Roche, 12156792910) according to manufacturer's protocol. Mounting medium with DAPI (UltraCruzTM, Santa Cruz Biotechnology, sc-24941) was placed over the tissue followed by a coverslip. Tile images were taken with an epifluorescent microscope (Zeiss Axio Imager M2, Zeiss, Germany). DAPI signal (blue) was overlayed with Texas Red ($TUNEL^+$ cells) and quantified using ImageJ to assess the number of $TUNEL^+$ cells overlapping with DAPI in the areas of interest.

Image quantification

Quantification of protein expression in tissue sections with immunofluorescent staining was performed using ImageJ software[45] (Fiji version 2.0.-rc-54/1.51g) The area of interest was circumscribed using the freehand selection tool and the image red, green, and blue channels were separated. Quantification was performed according to the color of the portion of interest and quantified as pixel density. The outcomes were normalized to the DAPI stained area of the corresponding image and results were presented as percentages (Antibody/ DAPI % density). For each analysis, 3-5 tissue sections from a minimum of three animals were used. mRNA quantification using RNAscope assay was performed by manual counting the mRNA events using ImageJ, as suggested by the manufacturer. Each punctuated red dot in the image represents one mRNA copy. For each experimental group, 3-6 sections from three animals were quantified.

Statistics

Quantitative results were reported as means **-/+** standard deviations. The normality of the data was assessed by Shapiro-Wilk test. Depending on the normality, either Student's t-test or

Mann–Whitney U test was performed to compare the means between the anti-TNF-α group and the control group. One-way and two-way ANOVA were performed in data sets containing multiple variables, followed with Holm-Sidak pairwise multiple comparison correction test. Analyses were performed using R Studio (Boston, MA). Statistical significance was set at $P < 0.05$ (2-tail).

Figure legend

Figure 1. Limbal cell apoptosis triggered after central ocular alkali burn caused severe limbal stem cell deficiency and complete corneal conjunctivalization.

(A) Biomicroscopic photo of a rabbit cornea immediately after 20 seconds of central 8-mm diameter alkali burn (NaOH 2N). **(B, C)** Limbal and peripheral corneal cell apoptosis 2 weeks after the injury using immunochistochemistry (IHC) and TUNEL assay. **(D)** Quantification of $TUNEL^+$ cells. **(E, F)** Representative biomicroscopic photos of rabbit limbus showing severe neovascularization and opacification of the cornea 2 weeks after the injury. **(G, K)** Phenotypical appearance of C57BL/6 mouse eye 2 weeks after central corneal alkali burn. **(H-J, L-N)** IHC analysis of tissue sections and flat mounts of naive and alkali injured mouse corneas using K12 (green) and K13 (red) markers, at 1.5 and 8 months post injury. **(O)** Immunofluorescent quantification of $K12^+$ / $K13^+$ expression 8 months after central corneal alkali burn.

(D) n=3 rabbits/group, ***$P<0.001$,* unpaired T test, two-tailed, equal variance. **(O)** n=4 mice/ group, **$P<0.01$; unpaired T test, two-tailed, equal variance. All data expressed as means ± SD.

K12: cytokeratin-12, **K13**: cytokeratin-13, **per.cornea**: peripheral cornea.

Figure 2. Anterior chamber pH elevation without ocular surface injury leads to LSC loss.

(A, D) Phenotypical appearance of C57BL/6 mouse eye at one month after intracameral injection of 11.4 or 7.4 pH balanced salt solution (pH normalizes within 30-45 minutes)[9]. **(B-F)** Representative immunofluorescent staining (confocal maximum projection) of ABCB5 expressing limbal stem cells (green) of cannulated eyes at 3 months. **(G)** Quantification of $ABCB5^{+}$ cells. **(H)** Representative photo of the anterior chamber cannulation procedure using small glass capillary.

n= 3 mice/group, *$P<0.05$; unpaired T test, two-tailed, equal variance. All data expressed as means ± SD. **LSC**: limbal epithelial stem cell, **AC**: anterior chamber, **Conj.**: conjunctiva, **ABCB5**: ATP-binding cassette sub-family B member 5.

Figure 3. Blood-derived monocyte infiltration into the cornea after central corneal burn.

(A-C) Representative flow cytometric plots and quantification of $CD45^{+}$ cells from $CX3CR1^{+/EGFP}$::$CCR2^{+/RFP}$ reporter mice 24 hours after corneal alkali injury. **(D-F)** Representative confocal images and quantification of $CX3CR1^{+/EGFP}$ and $CCR2^{+/RFP}$ cell infiltration in the cornea/limbus 7 days after corneal alkali injury in $CX3CR1^{+/EGFP}$::$CCR2^{+/RFP}$ reporter mice. **(G-I)** Immunohistochemistry (IHC) and quantification of cornea/limbus $CD45^{+}$ cells 3 months after alkali injury in rabbit eyes.

n=3 animals/group, *$P<0.05$, **$P<0.01$, ***$P<0.001$, unpaired T test, two-tailed, equal variance. **CCR2**: C-C chemokine receptor type 2, **CX3CR1**:CX3C chemokine receptor 1.

Figure 4. Blood-derived monocyte infiltration in the limbus promote TNF-α-mediated LSC death.

Animals received central corneal alkali burn (NaoH 1N) for 20 seconds[9] and tissues were collected and analyzed 24 hours later. **(A-C)** Representative flow cytometry histograms and quantification of TNF-α expression from $CCR2^{+}$ and $CX3CR1^{+}$ cells. **(D, E, G, H, J, K)** Representative bright field images and quantification of spatial distribution of TNF-α mRNA transcripts in the limbus and peripheral cornea of mice 24 hours after injury using RNA-scope. Red dots represent TNF-α mRNA transcript. **(F, I, L, M)** Representative immunofluorescent images and quantification of TNF-α protein expression in limbus and cornea of mice 24 hours after injury.

(C) n=3 mice/group, two-way ANOVA analysis with Sidak's correction. **(J-L)** n=3 animals/ group, unpaired T test, two-tailed, equal variance. All data expressed as means ± SD. ***P<0.01, ***P<0.001*, *****P<0.0001*

Figure 5. Increased presence of $CCR2^{+/RFP}$ blood-derived monocytes as compared to $CX3CR1^{+/EGFP}$ resident macrophages in the limbus associated with severe limbal cell death.

Bone marrow transferred animals received small-molecule CSF1R inhibitor PLX5622 for 3 weeks followed by central cornea alkali burn with NaOH 1N. Tissues were collected and analyzed at various time points post injury. **(A-F)** Representative flat mount confocal images and quantification of $CX3CR1^{+/EGFP}$ :: $CCR2^{+/RFP}$ bone marrow chimeras under different treatment conditions, including tissue-resident macrophages depletion using PLX5622 (PLX). **(G-L)** TUNEL assay and quantification of cell apoptosis 24 hours after corneal alkali injury in wild-

type mice under different treatment conditions, including PLX treatment. **(M-O)** Ex-vivo assessment of cornea-limbus cell apoptosis after incubation with 5 ng/mL murine TNF-α for 6 hours in *ex vivo* cultures. Wild-type mice were either naive or pre-treated with PLX5622 for 3 weeks to deplete their tissue-resident macrophages.

(L) n= 3 mice/group, one-way ANOVA with Turkey's correction. **(N)** n=5 animals/group, one-way ANOVA with Holm-Sidak's correction. All data expressed as means ± SD. *$P<0.05$, **$P<0.01$, ***$P<0.001$, ****$P<0.0001$. **BMT**: bone marrow transfer, **PLX** : Plexxikon 5622.

Figure 6. Tissue-resident macrophages in the cornea acquire a protective signature following exposure to TNF-α.

Ex-vivo assessment of the phenotype of corneal tissue-resident macrophages following exposure to 5 ng/mL murine TNF-α for 6 hours. **(A, B)** Representative flow cytometric plots and quantification at 24 hours and 2 months of classical and alternative polarization markers expressed by corneal tissue-resident macrophages following *ex vivo* exposure to recombinant TNF-α (rTNF-α) with and without exposure to CSF1R inhibitor. **(B)** Exposure of explanted corneas to rTNF-α alters the polarization of $CX3CR1^{+}$ tissue resident macrophages from MHC-II^{hi} $CD86^{+}$ $CD206^{-}$ (classical activation) to MHC-II^{lo} $CD86^{-}$ $CD206^{+}$ (alternative activation). This phenotype switch is lost in mice treated with CSF1R inhibitor for macrophage depletion. Repopulation of tissue-resident macrophages after cessation of the CSF1R inhibitor for 2 month re-establishes the phenotype switch upon exposure to rTNF-α. n= 4 mice/group, *$P<0.05$,****$P<0.0001$, one-way ANOVA, Dunnett's multiple comparison test, all comparisons to CTRL group.

Figure 7. **Proposed mechanism of limbal epithelial stem cell loss after central corneal alkali burn injury.**

Rapid pH elevation in the aqueous humor causes uveal stress and subsequent infiltration of peripheral monocytes into the basal limbal tissue. In contrast to tissue-resident macrophages, peripheral monocytes secretory significant amount of TNF-α that causes limbal stem cell death. Prompt TNF-α inhibition after injury reduces monocyte infiltration into the limbus, suppresses inflammation, protects the limbal stem cell from apoptosis and preserved the ocular surface phenotype.

Bibliography

1. C. H. Dohlman, F. Cade, R. Pfister, Chemical burns to the eye: paradigm shifts in treatment. *Cornea* **30**, 613-614 (2011).
2. H. S. Dua, J. A. Gomes, A. Singh, Corneal epithelial wound healing. *The British Journal of Ophthalmology* **78**, 401-408 (1994).
3. R. A. Thoft, J. Friend, The X, Y, Z hypothesis of corneal epithelial maintenance. *Investigative Ophthalmology & Visual Science* **24**, 1442-1443 (1983).
4. S. S. Shanbhag, H. N. Saeed, E. I. Paschalis, J. Chodosh, Keratolimbal allograft for limbal stem cell deficiency after severe corneal chemical injury: a systematic review. *British Journal of Ophthalmology* 10.1136/bjophthalmol-2017-311249 (2017).
5. K. A. Williams *et al.*, Use of DNA Polymorphisms and the Polymerase Chain Reaction to Examine the Survival of a Human Limbal Stem Cell Allograft. *American Journal of Ophthalmology* **120**, 342-350 (1995).
6. M. S. Santos *et al.*, Survival Analysis of Conjunctival Limbal Grafts and Amniotic Membrane Transplantation in Eyes With Total Limbal Stem Cell Deficiency. *American Journal of Ophthalmology* **140**, 223.e221-223.e229 (2005).
7. J. Shimazaki, H.-Y. Yang, K. Tsubota, Amniotic Membrane Transplantation for Ocular Surface Reconstruction in Patients with Chemical and Thermal Burns. *Ophthalmology* **104**, 2068-2076 (1997).
8. F. Cade *et al.*, Alkali burn to the eye: protection using TNF-α inhibition. *Cornea* **33**, 382-389 (2014).
9. E. I. Paschalis *et al.*, Mechanisms of Retinal Damage after Ocular Alkali Burns. *The American journal of pathology* **187**, 1327-1342 (2017).
10. C. Zhou *et al.*, Sustained Subconjunctival Delivery of Infliximab Protects the Cornea and Retina Following Alkali Burn to the Eye. *Investigative ophthalmology & visual science* **58**, 96-105 (2017).
11. B. R. Ksander *et al.*, ABCB5 is a limbal stem cell gene required for corneal development and repair. *Nature* **511**, 353-357 (2015).
12. E. I. Paschalis *et al.*, The Role of Microglia and Peripheral Monocytes in Retinal Damage after Corneal Chemical Injury. *The American journal of pathology* **188**, 1580-1596 (2018).
13. E. I. Paschalis *et al.*, Permanent neuroglial remodeling of the retina following infiltration of CSF1R inhibition-resistant peripheral monocytes. *Proceedings of the National Academy of Sciences of the United States of America* **115**, E11359-E11368 (2018).
14. G. Ferrari, F. Bignami, C. Giacomini, S. Franchini, P. Rama, Safety and Efficacy of Topical Infliximab in a Mouse Model of Ocular Surface ScarringSafety and Efficacy of Topical Infliximab. *Investigative ophthalmology & visual science* **54**, 1680-1688 (2013).
15. F. Cade *et al.*, Alkali Burn to the Eye: Protection Using TNF-α Inhibition. *Cornea* **33**, 382-389 (2014).
16. E. I. Paschalis *et al.*, Mechanisms of Retinal Damage after Ocular Alkali Burns. *The American Journal of Pathology* **187**, 1327-1342 (2017).

17. F. Lei *et al.*, CSF1R inhibition by a small-molecule inhibitor is not microglia specific; affecting hematopoiesis and the function of macrophages. *Proc Natl Acad Sci U S A* 10.1073/pnas.1922788117 (2020).
18. F. Lei *et al.*, Reply to Green and Hume: Nonmicroglia peripheral immune effects of short-term CSF1R inhibition with PLX5622. *Proceedings of the National Academy of Sciences of the United States of America* **118** (2021).
19. N. N. Dagher *et al.*, Colony-stimulating factor 1 receptor inhibition prevents microglial plaque association and improves cognition in 3xTg-AD mice. *Journal of neuroinflammation* **12**, 139 (2015).
20. E. I. Paschalis *et al.*, Microglia Regulate Neuroglia Remodeling in Various Ocular and Retinal Injuries. *Journal of immunology (Baltimore, Md. : 1950)* **202**, 539-549 (2019).
21. K. M. Hatch, R. Dana, The structure and function of the limbal stem cell and the disease states associated with limbal stem cell deficiency. *Int Ophthalmol Clin* **49**, 43-52 (2009).
22. W. F. Hughes, Jr., Alkali burns of the eye; review of the literature and summary of present knowledge. *Arch Ophthal* **35**, 423-449 (1946).
23. M. F. Goldberg, A. Bron, Limbal palisades of Vogt. *Transactions of the American Ophthalmological Society* **80**, 155 (1982).
24. R. Schofield, The stem cell system. Biomedicine & pharmacotherapy= Biomedecine & pharmacotherapie **37**, 375-380 (1983).
25. S. C. Tseng, Regulation and clinical implications of corneal epithelial stem cells. *Molecular biology reports* **23**, 47-58 (1996).
26. J. M. Wolosin, X. Xiong, M. Schutte, Z. Stegman, A. Tieng, Stem cells and differentiation stages in the limbo-corneal epithelium. *Prog Retin Eye Res* **19**, 223-255 (2000).
27. M. A. Dziasko, J. T. Daniels, Anatomical Features and Cell-Cell Interactions in the Human Limbal Epithelial Stem Cell Niche. *Ocul Surf* **14**, 322-330 (2016).
28. L. Arnold *et al.*, Inflammatory monocytes recruited after skeletal muscle injury switch into antiinflammatory macrophages to support myogenesis. *The Journal of experimental medicine* **204**, 1057-1069 (2007).
29. M. Burgess, K. Wicks, M. Gardasevic, K. A. Mace, Cx3CR1 Expression Identifies Distinct Macrophage Populations That Contribute Differentially to Inflammation and Repair. *ImmunoHorizons* **3**, 262-273 (2019).
30. C. Vestergaard, H. Just, J. Baumgartner Nielsen, K. Thestrup-Pedersen, M. Deleuran, Expression of CCR2 on Monocytes and Macrophages in Chronically Inflamed Skin in Atopic Dermatitis and Psoriasis. *Acta Dermato-Venereologica* **84**, 353-358 (2004).
31. S. Goyal, S. K. Chauhan, Q. Zhang, R. Dana, Amelioration of murine dry eye disease by topical antagonist to chemokine receptor 2. *Arch Ophthalmol* **127**, 882-887 (2009).
32. G. Ren *et al.*, CCR2-Dependent Recruitment of Macrophages by Tumor-Educated Mesenchymal Stromal Cells Promotes Tumor Development and Is Mimicked by TNFα. *Cell Stem Cell* **11**, 812-824 (2012).
33. S. Willenborg *et al.*, CCR2 recruits an inflammatory macrophage subpopulation critical for angiogenesis in tissue repair. *Blood* **120**, 613-625 (2012).

34. F. Sennlaub *et al.*, CCR2(+) monocytes infiltrate atrophic lesions in age-related macular disease and mediate photoreceptor degeneration in experimental subretinal inflammation in Cx3cr1 deficient mice. *EMBO molecular medicine* **5**, 1775-1793 (2013).
35. T. A. Evans *et al.*, High-resolution intravital imaging reveals that blood-derived macrophages but not resident microglia facilitate secondary axonal dieback in traumatic spinal cord injury. *Experimental neurology* **254**, 109-120 (2014).
36. J. Han *et al.*, Underestimated Peripheral Effects Following Pharmacological and Conditional Genetic Microglial Depletion. *Int J Mol Sci* **21** (2020).
37. C. H. Dohlman *et al.*, Glaucoma After Corneal Trauma or Surgery—A Rapid, Inflammatory, IOP-Independent Pathway. *Cornea* 10.1097/ICO.0000000000002106, 1-2 (2019).
38. R. J.-F. Tsai, S. C. Tseng, Human allograft limbal transplantation for corneal surface reconstruction. *Cornea* **13**, 389-400 (1994).
39. S. C. Tseng, P. Prabhasawat, K. Barton, T. Gray, D. Meller, Amniotic membrane transplantation with or without limbal allografts for corneal surface reconstruction in patients with limbal stem cell deficiency. *Archives of Ophthalmology* **116**, 431-441 (1998).
40. K. Tsubota *et al.*, Treatment of severe ocular-surface disorders with corneal epithelial stem-cell transplantation. *New England Journal of Medicine* **340**, 1697-1703 (1999).
41. P. Rama *et al.*, AUTOLOGOUS FIBRIN-CULTURED LIMBAL STEM CELLS PERMANENTLY RESTORE THE CORNEAL SURFACE OF PATIENTS WITH TOTAL LIMBAL STEM CELL DEFICIENCY1. *Transplantation* **72** (2001).
42. J. A. P. Gomes, M. S. dos Santos, M. C. Cunha, J. de Nadai Barros, L. B. de Sousa, Amniotic membrane transplantation for partial and total limbal stem cell deficiency secondary to chemical burn. *Ophthalmology* **110**, 466-473 (2003).
43. A. J. Shortt *et al.*, Ex Vivo Expansion and Transplantation of Limbal Epithelial Stem Cells. *Ophthalmology* **115**, 1989-1997 (2008).
44. X. Chen *et al.*, Glaucoma after ocular surgery or trauma: the role of infiltrating monocytes and their response to cytokine inhibitors. *The American journal of pathology* 10.1016/j.ajpath.2020.07.006 PMID - 32693061 (2020).
45. J. Schindelin *et al.*, Fiji: an open-source platform for biological-image analysis. *Nature methods* **9**, 676-682 (2012).

Figure 1. Limbal cell apoptosis triggered after central ocular alkali burn caused severe limbal stem cell deficiency and complete corneal conjunctivalization.

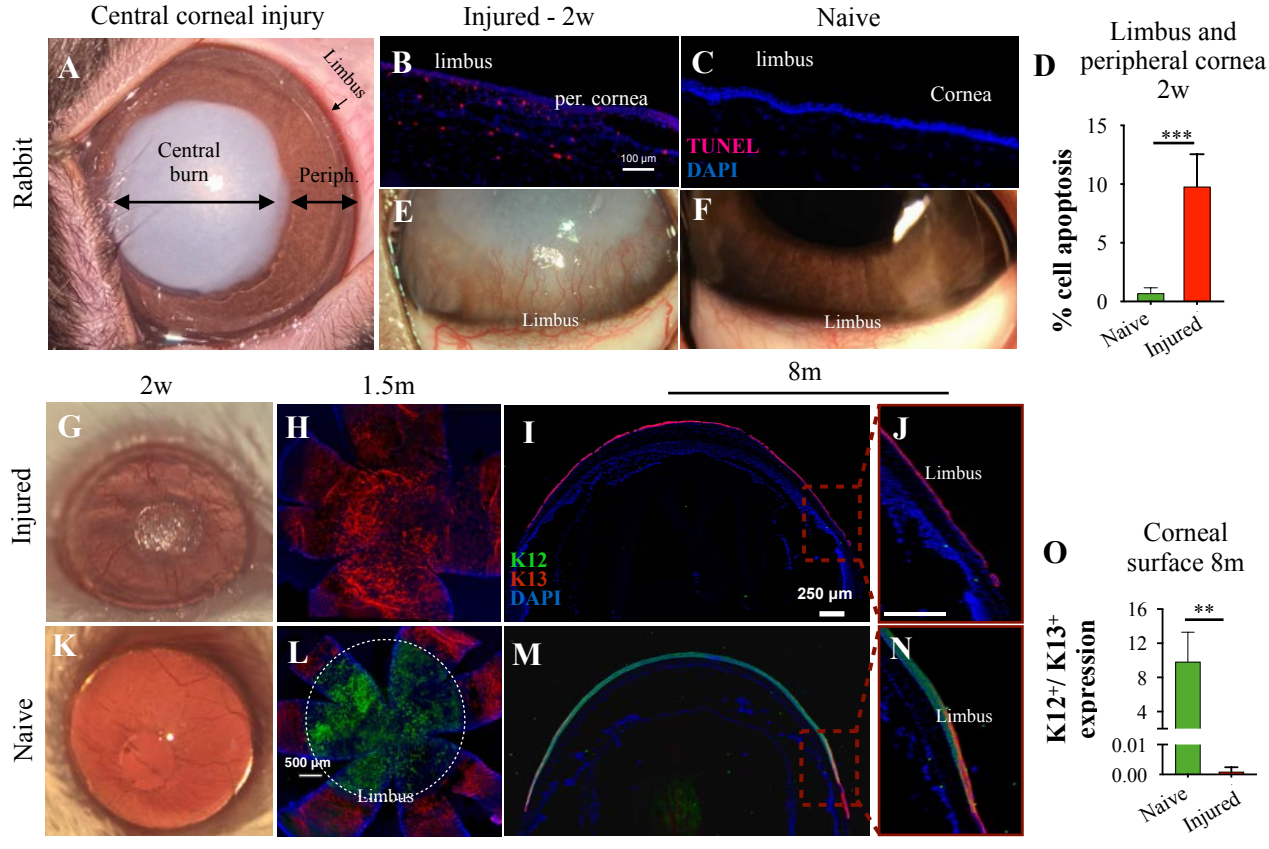

Figure 2. Anterior chamber pH elevation without ocular surface injury leads to LSC loss.

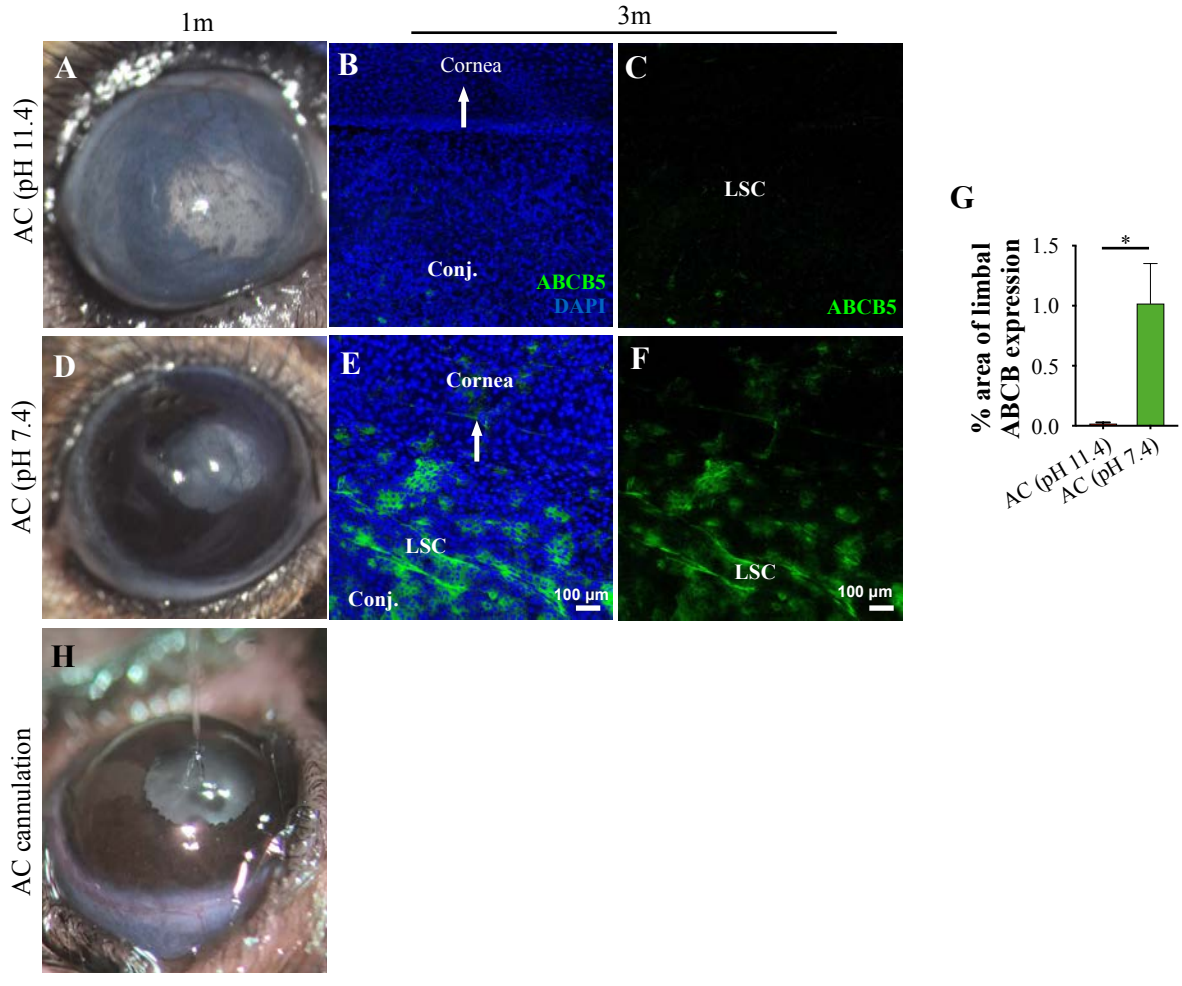

Figure 3. Blood-derived monocyte infiltration into the cornea after central corneal burn.

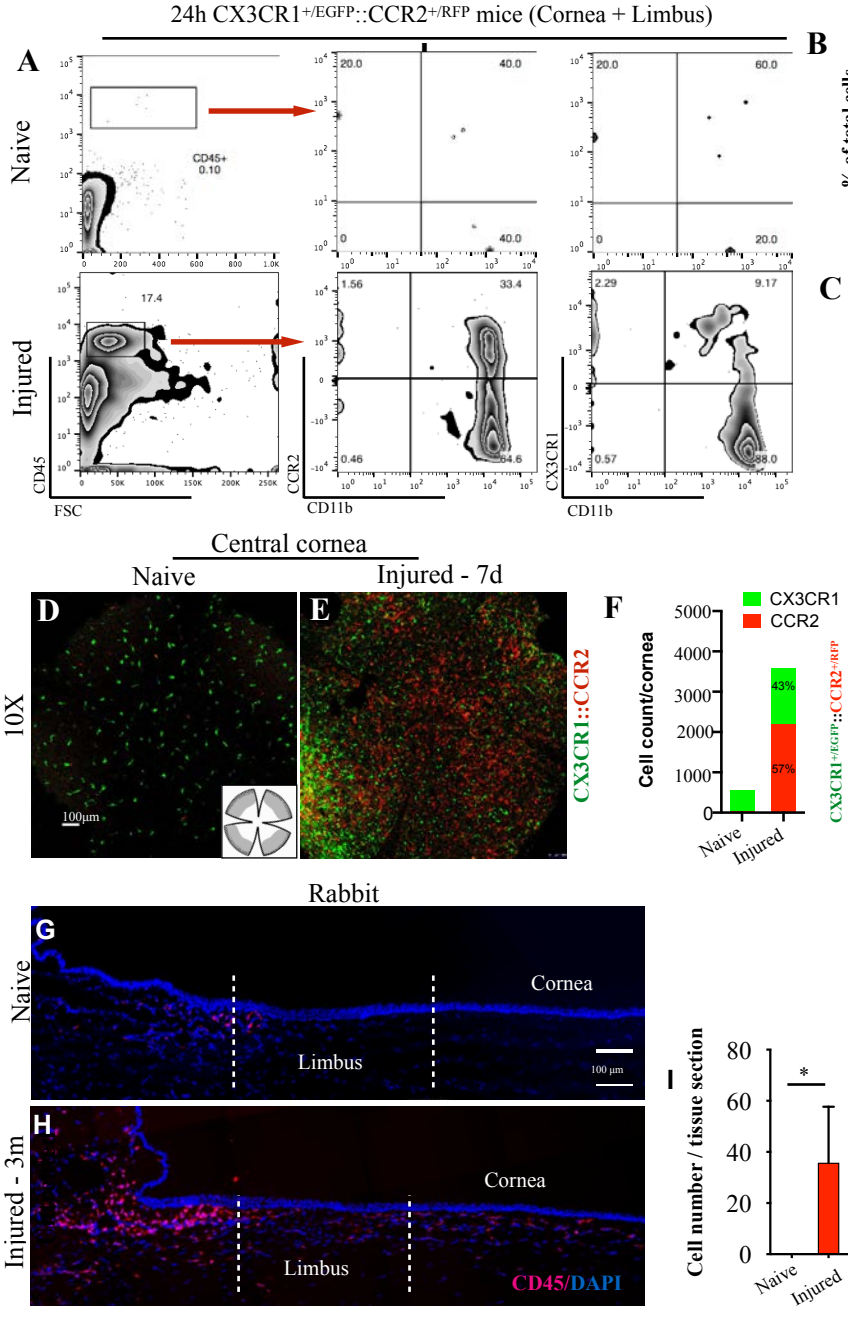

Figure 4. Blood-derived monocyte infiltration in the limbus promote TNF-α-mediated LSC death.

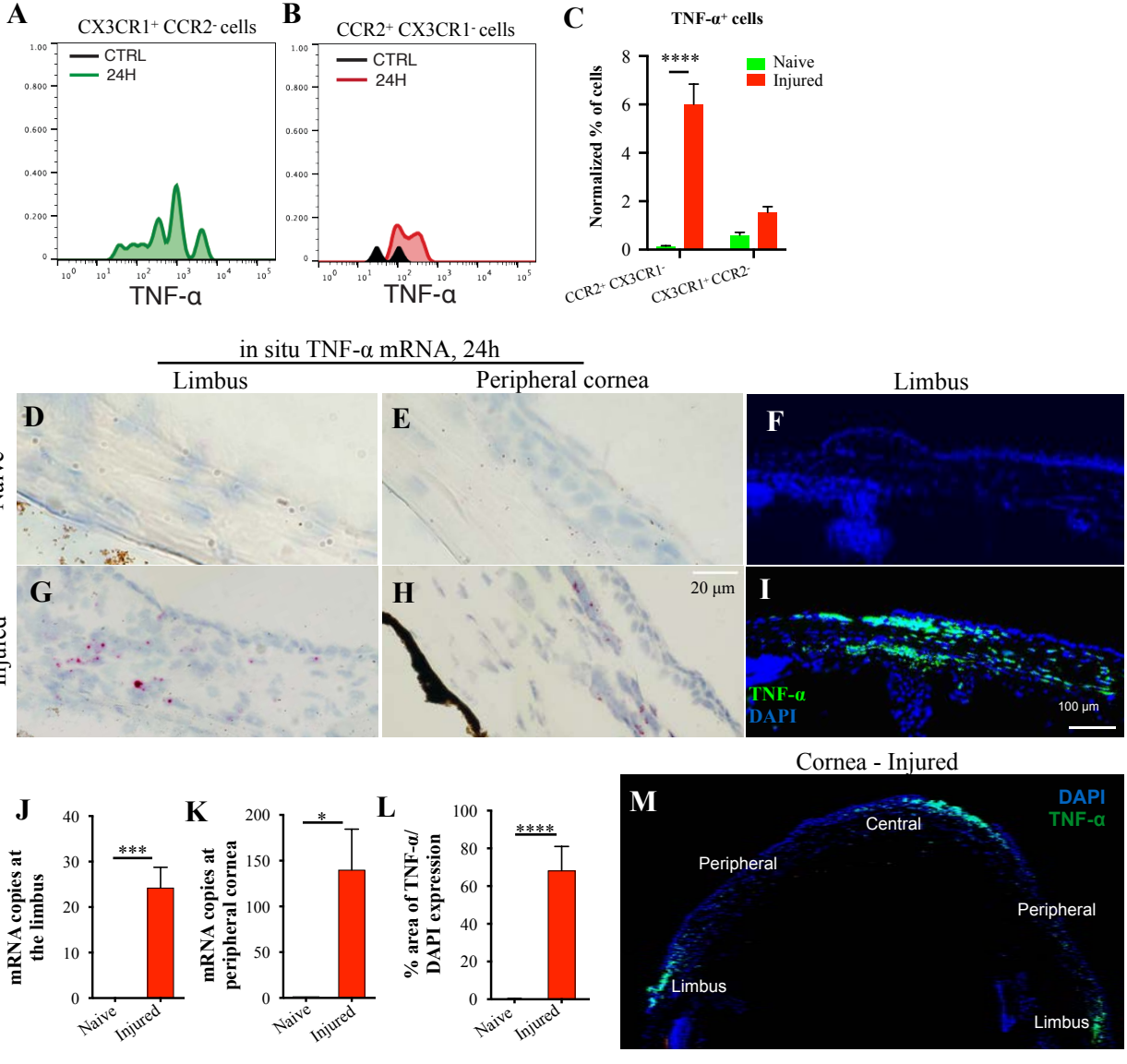

Figure 5. Increased presence of CCR2$^{+/RFP}$ blood-derived monocytes as compared to CX3CR1$^{+/EGFP}$ resident macrophages in the limbus was associated with severe limbal cell death following alkali injury.

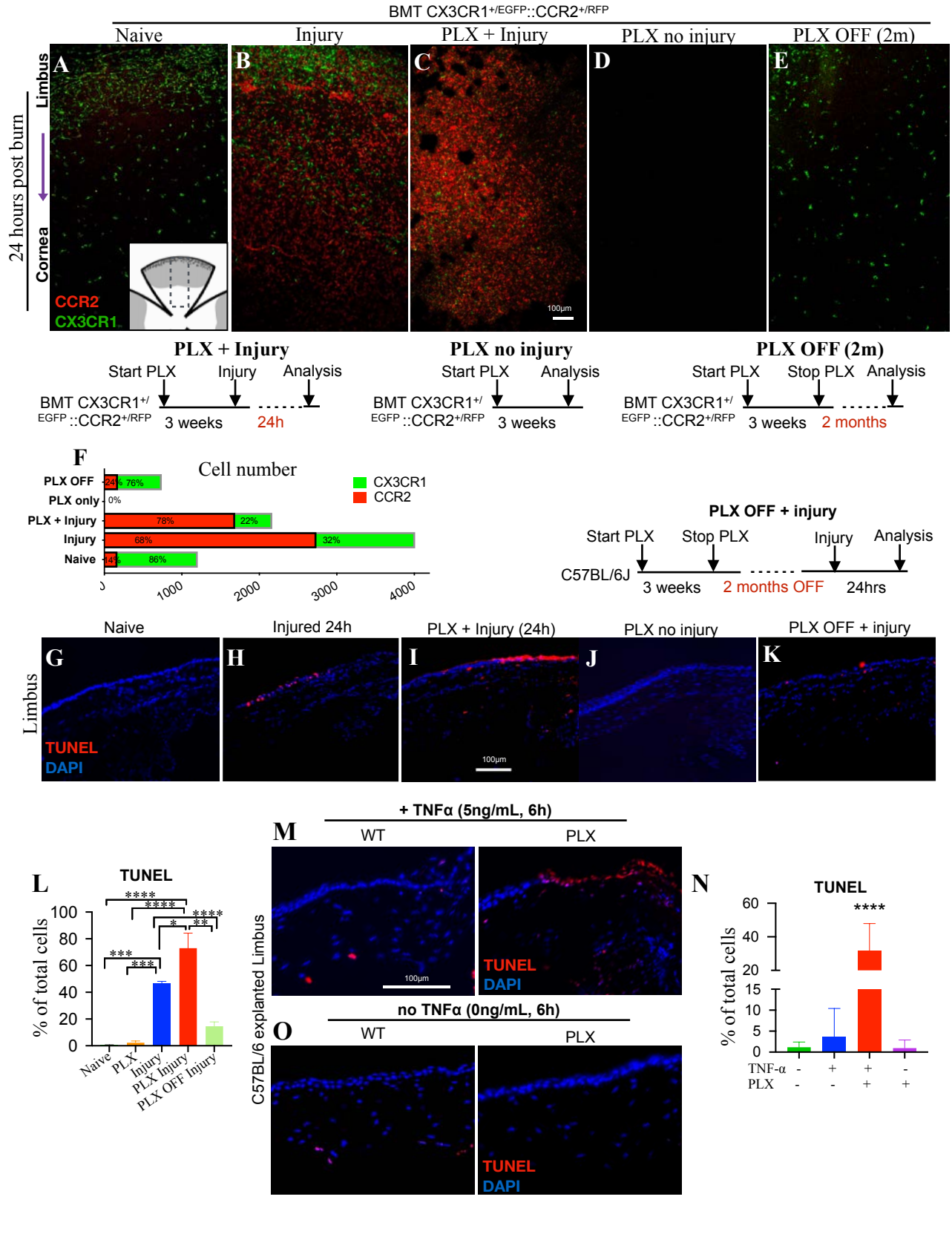

Figure 6. Tissue-resident macrophages in the cornea acquire a protective signature following exposure to TNF-α.

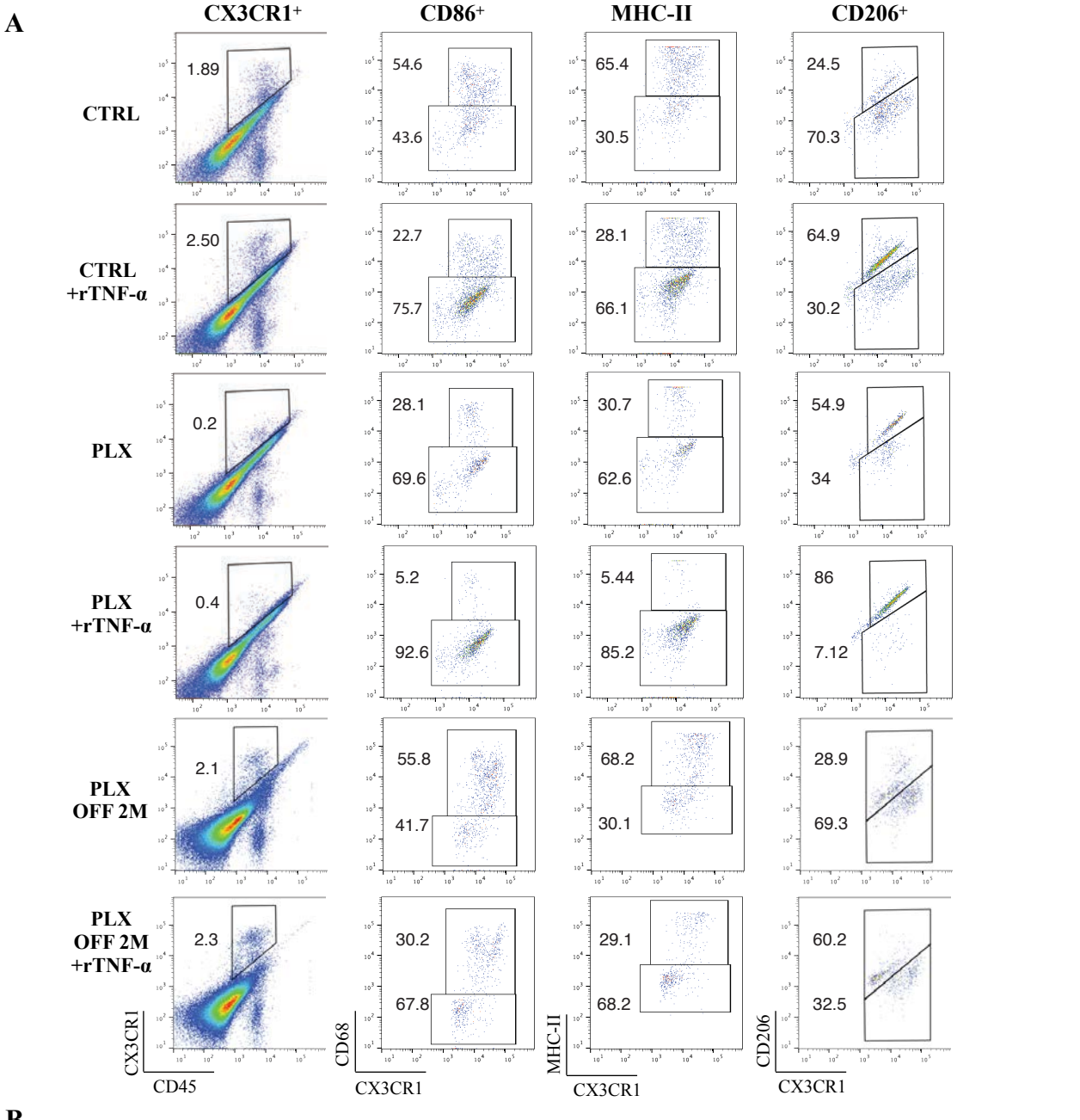

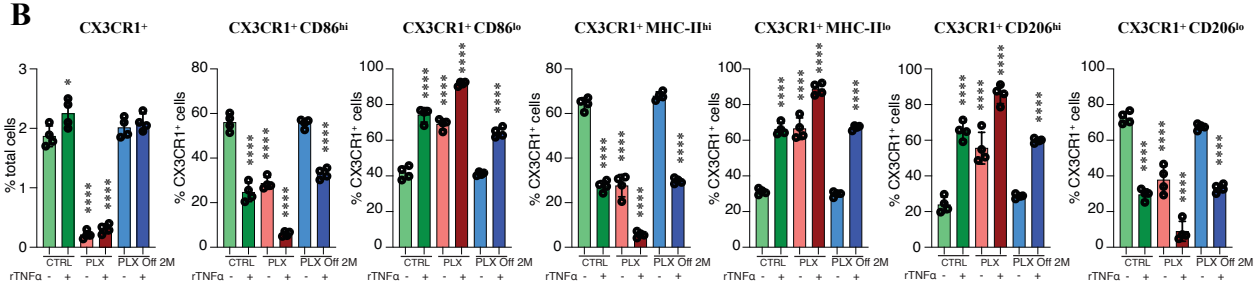

M1 phenotype: MHC-II^{hi} CD86^{+} CD206^{-}
M2 phenotype: MHC-II^{lo} CD86^{-} CD206^{+}

Figure 7. Proposed mechanism of limbal epithelial stem cell loss after central corneal alkali burn injury.